The crystal structure of a triacylglycerol lipase from *Pseudomonas cepacia* reveals a highly open conformation in the absence of a bound inhibitor

Kyeong Kyu Kim[†], Hyun Kyu Song, Dong Hae Shin[‡], Kwang Yeon Hwang[§] and Se Won Suh*

Background: Lipases, a family of enzymes which catalyze the hydrolysis of triglycerides, are widely distributed in many organisms. True lipases are distinguished from esterases by the characteristic interfacial activation they exhibit at an oil–water interface. Lipases are one of the most frequently used biocatalysts for organic reactions performed under mild conditions. Their biotechnological applications include food and oil processing and the preparation of chiral intermediates for the synthesis of enantiomerically pure pharmaceuticals. Recent structural studies on several lipases have provided some clues towards understanding the mechanisms of hydrolytic activity, interfacial activation, and stereoselectivity. This study was undertaken in order to provide structural information on bacterial lipases, which is relatively limited in comparison to that on the enzymes from other sources.

Results: We have determined the crystal structure of a triacylglycerol lipase from *Pseudomonas cepacia* (PcL) in the absence of a bound inhibitor using X-ray crystallography. The structure shows the lipase to contain an α/β-hydrolase fold and a catalytic triad comprising of residues Ser87, His286 and Asp264. The enzyme shares several structural features with homologous lipases from *Pseudomonas glumae* (PgL) and *Chromobacterium viscosum* (CvL), including a calcium-binding site. The present structure of PcL reveals a highly open conformation with a solvent-accessible active site. This is in contrast to the structures of PgL and PcL in which the active site is buried under a closed or partially opened 'lid', respectively.

Conclusions: PcL exhibits some structural features found in other lipases. The presence of the Ser-His-Asp catalytic triad, an oxyanion hole, and the opening of a helical lid suggest that this enzyme shares the same mechanisms of catalysis and interfacial activation as other lipases. The highly open conformation observed in this study is likely to reflect the activated form of the lipase at an oil–water interface. The structure suggests that the interfacial activation of bacterial lipases involves the reorganization of secondary structures and a large movement of the lid to expose the active site. This is similar to the mechanism described for other well characterized fungal and mammalian lipases.

Address: Department of Chemistry, College of Natural Sciences, Seoul National University, Seoul 151-742, Korea.

Present addresses: [†]Department of Chemistry, University of California, Berkeley, CA 94720, USA, [‡]Protein Engineering Research Division, Korea Research Institute of Bioscience and Biotechnology, KIST, P.O. Box 115, Yusung, Taejon 305-600, Korea and [§]MRC Group in Protein Structure and Function, Department of Biochemistry, University of Alberta, Edmonton, Alberta T6G 2H7, Canada.

*Corresponding author.
E-mail: sewonsuh@plaza.snu.ac.kr

Key words: lipase, *Pseudomonas cepacia*, X-ray structure

Received: 30 September 1996
Revisions requested: 25 October 1996
Revisions received: 11 November 1996
Accepted: 4 December 1996

Electronic identifier: 0969-2126-005-00173

Structure 15 February 1997, 5:173–185

Introduction

Triacylglycerol lipases (EC 3.1.1.3), present in diverse organisms including animals, plants, fungi, and bacteria, catalyze the hydrolysis of triglycerides into free fatty acids and glycerol. They show a wide range of molecular sizes, substrate and positional specificities, and catalytic rates [1]. A unique property of true lipases that distinguishes them from esterases is their enhanced activity at an oil–water interface (interfacial activation).

Lipases are widely used for industrial purposes. They are efficient stereoselective catalysts in the kinetic resolution of a wide variety of chiral compounds [2] and are useful in transesterification, synthesis of esters and peptides, and resolution of racemic mixtures to produce various optically active compounds [2,3]. Several organochemical and crystallographic studies have provided some insight into their enantioselectivity [4–7]. On the basis of these studies, a general rule for the enantiopreference towards the production of a secondary alcohol, and the positioning of the scissile fatty acid chain and ester bond has been proposed [4–6].

The structures of many different lipases have been determined by X-ray crystallography: fungal lipases from *Rhizomucor miehei* [8], *Geotrichum candidum* [9,10], *Candida*

Figure 1

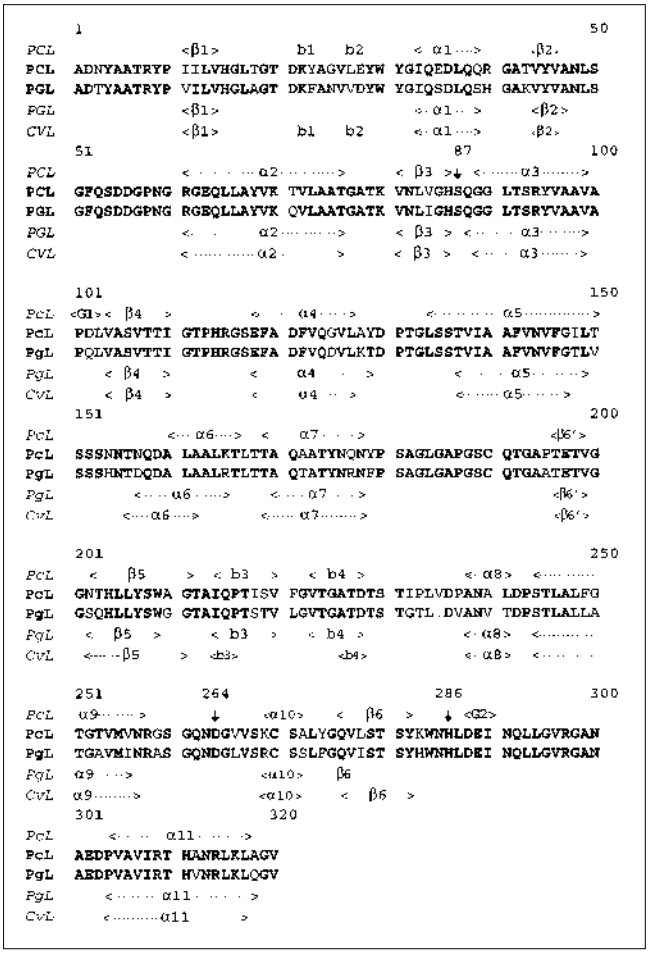

A comparison of amino acid sequences and secondary structure assignments of *P. cepacia* lipase (PcL), *P. glumae* lipase (PgL), and *C. viscosum* lipase (CvL); PgL and CvL have an identical amino acid sequence. The secondary structures, as defined by PROCHECK [58], are numbered according to [18]; G1 and G2 denote 3_{10} helices. Conserved residues are in bold and the three catalytic residues, Ser87, Asp265, and His287, are marked by arrows.

rugosa [11], *Humicola lanuginosa* [12], *Penicillium camembertii* [12], *Rhizopus delemar* [12], and *Candida antarctica* [13]; mammalian pancreatic lipases [14–16]; and bacterial lipases from *Pseudomonas glumae* [17] and *Chromobacterium viscosum* [18]. The amino acid sequences of the latter two lipases are identical [19]. Lipases are, in general, highly variable in size and the sequence similarity between them is limited to short spans located around the active-site residues. However, the three-dimensional structures of lipases, in their cores, share a common fold motif, known as an α/β-hydrolase fold [20]. This α/β-hydrolase fold has been identified in many other distantly or closely-related enzymes, including dienelactone hydrolase from *Pseudomonas sp.* B13 [21], acetylcholinesterase from *Torpedo californica* [22], haloalkane dehalogenase from *Xanthobacter autotrophicus* [23], carboxypeptidase II from wheat [24], cutinase from *Fusarium solani* [25], thioesterase from *Vibrio harveyi* [26], and cholesterol esterase from *Candida cylindracea* [27]. The general α/β-hydrolase fold consists of an eight-stranded, mostly parallel β sheet flanked by six α helices, with a catalytic triad (Ser/Asp/Cys-His-Asp/Glu). One of the most conserved features of the α/β-hydrolase enzymes is the nucleophile elbow, a sharp γ turn containing the nucleophilic serine residue, positioned between a β strand and an α helix.

Insights into the mechanism of catalysis, including the process of interfacial activation, have been provided by the crystal structures of lipases, both on their own and in complex with inhibitors. In the so-called 'closed' structures, the catalytic triad is buried underneath a helical segment, called a 'lid' or a 'flap'. Crystallographic analysis of a fungal lipase–inhibitor complex [28] and a complex of human pancreatic lipase and its substrate analog [15] revealed an 'open' conformation of the enzyme. In these two complexes, when the inhibitor is bound, the active site becomes accessible to the solvent and a hydrophobic surface is exposed by the movement of the lid. Similar open conformations have been observed in lipases from *C. rugosa* and *C. antarctica* (CrL and CaL) [13,29]. The conformational changes range from a simple rigid body hinge-type motion to complex reorganizations involving changes in the secondary structures. Generally speaking, these structural studies suggest that the hydrophobic lipid-binding site is opened up by the rolling back of the lid from the active site at an oil–water interface. However, even in the absence of an oil–water interface, there may be a subtle equilibrium between the two conformations of the enzyme. It is believed that the opening of the lid is essential but not sufficient to explain the interfacial activation [30].

The lipase from *Pseudomonas cepacia* (PcL) has been cloned [31,32], characterized [33–37], and crystallized [34, 37,38]. *P. cepacia* lipase shows a high preference for the hydrolysis of triglycerides with a chain length ≥ eight [37]. This enzyme is widely used for organic synthesis and hydrolysis because of its enantioselectivity [4,39]. Its amino acid sequence has been deduced from the cDNA sequence [31]. The mature polypeptide chain consists of 320 amino acid residues with a calculated molecular mass of 33 128 Da and its sequence is highly homologous to that of lipase from *P. glumae* (PgL) [40], with 84% sequence identity (Fig. 1). The PcL sequence also shows sequence identity of 33% and 22% to lipases from *Pseudomonas fragi* and *Pseudomonas fluorescens* [41,42], respectively. The 3.0 Å crystal structure of PgL showed that the enzyme is composed of three domains, the largest of which contains a subset of the α/β-hydrolase fold and a calcium-binding site [17]. PgL was crystallized in a closed conformation and a candidate region for the lid was proposed [17]. This

Figure 2

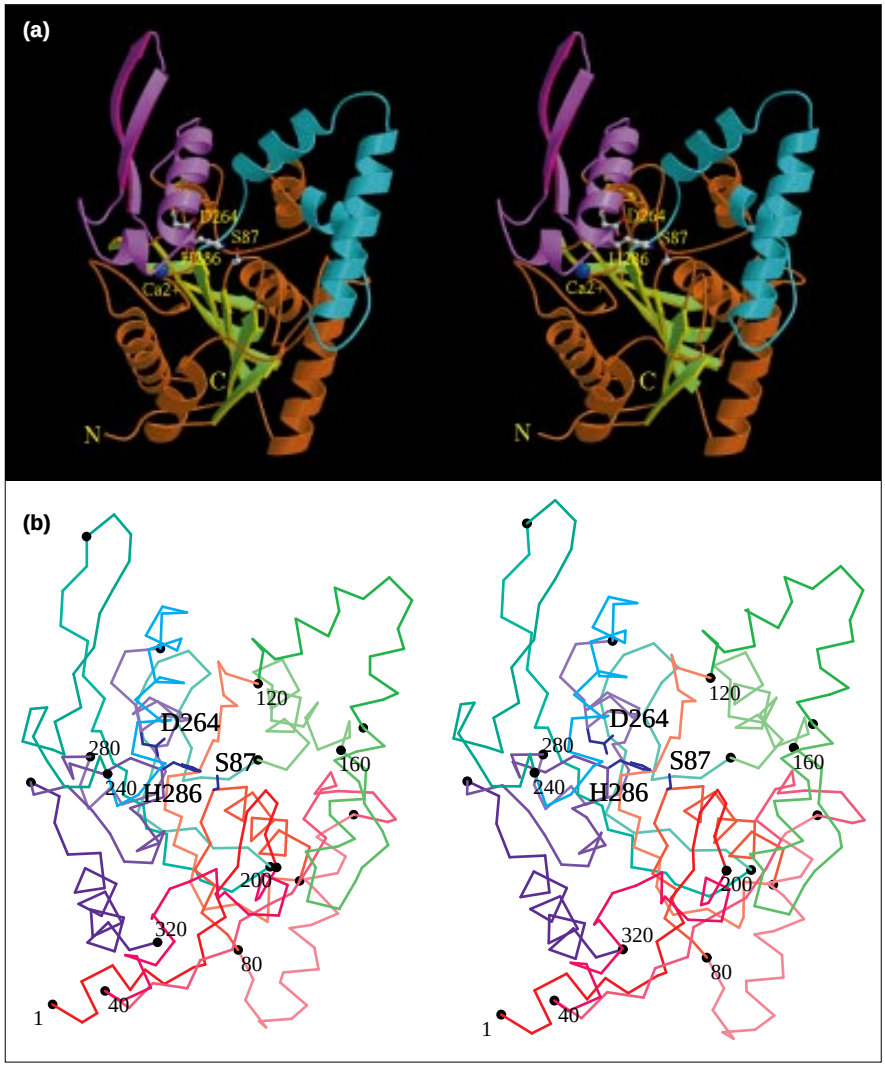

The overall fold of PcL. (**a**) Stereo ribbon diagram of PcL. The C domain is colored brown and green, U1 is colored blue, and U2 is purple. The N and C termini and the three catalytic residues are labeled; the catalytic residues are shown in ball-and-stick representation. The Ca^{2+} ion is shown as a dark blue sphere. (Figure drawn with MOLSCRIPT [60].) (**b**) A stereo view of the Cα trace of PcL; the catalytic residues are labeled and every twentieth residue is marked by dots.

region has recently been confirmed to form the lid by the 1.6 Å structure of *C. viscosum* lipase (CvL), in which the lid is partially opened [18].

In this study, the crystal structure of PcL determined by the multiple isomorphous replacement (MIR) method is reported. The structure shows for the first time a highly open conformation of a bacterial lipase, which is likely to represent the activated state of the enzyme at an oil–water interface.

Results and discussion

Overall structure

The crystal structure of a PcL has been determined in the absence of a bound inhibitor using the MIR method. There are two molecules of PcL in each asymmetric unit of the crystal and they are related to each other by a pure translation of x = 23.62 Å, y = 23.40 Å, z = 38.85 Å. The two molecules in the asymmetric unit are highly similar to each other and are superimposable with root mean square (rms) deviations of 0.14 Å and 0.30 Å for mainchain and sidechain atoms, respectively. Twelve residues (1, 74–76, 127, 131–133, 200, 220–222) show an rms deviation greater than 0.5 Å for the mainchain atoms and their B factors are higher than the average. In terms of the average B factors and B factor profiles, the two molecules in the asymmetric unit are not distinguishable from each other and thus, for the sake of convenience, one of them is arbitrarily chosen for the following discussion and comparisons, unless otherwise stated.

PcL is a globular enzyme with approximate dimensions of 30 Å × 40 Å × 50 Å and its structure may be divided into one large and two smaller domains (Fig. 2). The assignment of secondary structures of PcL and its comparison with homologs are shown in Figure 1, along with the sequence

Figure 3

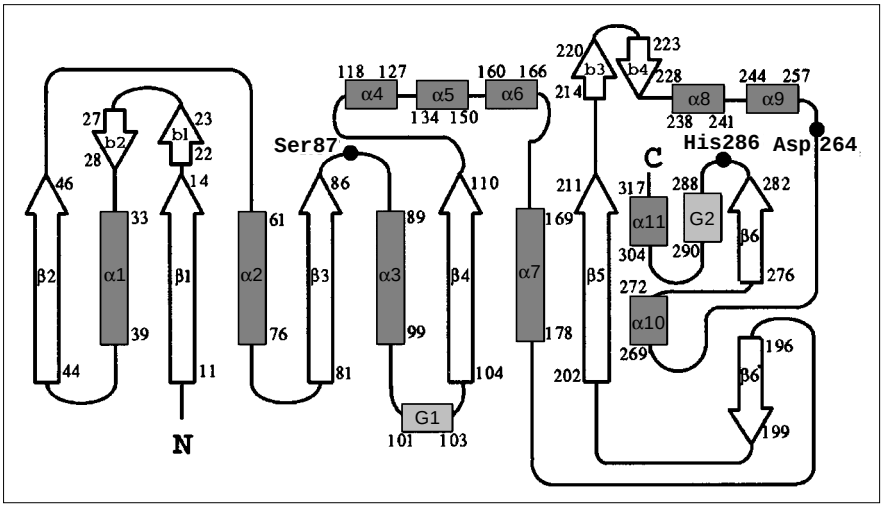

Topology diagram of PcL. The secondary structures are defined and labeled as in Figure 1; β strands are shown as arrows, α helices and 3_{10} helices (G1 and G2) are shown as rectangles. The three residues in the catalytic triad, Ser87, Asp264, and His286, are marked as black circles.

alignment. The numbering of helices and strands, following the nomenclature of CvL [18], is shown in the secondary structure diagram (Fig. 3).

The largest domain (C domain; residues 1–117, 167–214, and 262–320) consists of a central six-stranded parallel β sheet (β1, β2, β3, β4, β5, and β6) flanked by two α helices on one side (α1 and α11) and four α helices on the other (α2, α3, α7, and α10) (Figs 1–3). Its overall topology is very similar to the prototypic α/β-hydrolase fold in spite of little sequence homology to other members of this family. However, the first two β strands in the general α/β-hydrolase fold [19] are absent in this lipase. The first β strand (β1) of this lipase is, therefore, equivalent to β3 in the nomenclature of prototypic α/β-hydrolase fold enzymes [19]. Compared with the general α/β-hydrolase fold, there is an additional β strand (β6′ in Figs 1,3) which is lined up with the sixth strand (β6) in the central β sheet, but in the opposite direction. Helix α10, corresponding to helix E in the general α/β-hydrolase fold, is very short. A disulfide bond, between Cys190 and Cys270, cross-links α10 and a loop on the N-terminal side of β6′.

The second domain (U1 domain; residues 118–166) is composed of three α helices (α4, α5, and α6), and the third domain (U2 domain; residues 213–261) consists of two antiparallel β strands (β3 and β4) and two α helices (α8 and α9) (Fig. 3). The U1 domain is inserted between β4 and α7 of the main C domain, while the U2 domain is inserted between β5 and α10. This topological relationship among the three domains is common among many α/β-hydrolase fold enzymes. These two inserted domains in PcL are equivalent to those between β6 and αD, and between β7 and αE in the general α/β-hydrolase fold [19]. The inner faces of the U1 and U2 domains, and the C-terminal edge of the β strands from the C domain form the active-site cleft around the nucleophile Ser87 (Fig. 2).

A comparison with highly homologous lipase structures

The first crystal structure of a bacterial lipase to be reported was that of PgL at 3.0 Å resolution [17]. When the sequences of PcL and PgL are compared, there are fifty residues which differ between the two sequences and one insertion (Val235; Fig. 1). The assignments of secondary structures to both lipases are very similar (Fig. 1). However, despite an overall similarity in sequence and secondary structure, there are some large and significant differences in the tertiary structures of these two enzymes (Figs 4,5). Many of the large differences are due to the different conformations adopted by the enzymes in the different crystalline environments. For 265 structurally equivalent Cα atoms, out of 318 common Cα atoms in both lipases (excluding Val235, an inserted residue, and Ala1 which is missing from the PgL model), a superposition gives an rms deviation of 0.39 Å. For all 318 common Cα atoms, the rms deviation is 1.9 Å, as the most discrepant 53 Cα atoms (of residues 17–27, 50–52, 130–166, and 233–234) give a very large rms deviation of 9.4 Å.

The largest difference between PcL and PgL is observed for residues 130–166 (marked C in Fig. 5), which encompasses the two helices α5 and α6 of the U1 domain. Figure 4 shows the dramatic shift of helix α5, by as much as 20 Å, confirming the previous proposal that this helix acts as a lid in the PgL structure [17]. Besides the large shift in its position, helix α5 in PcL is longer than that of PgL by nearly one turn. This is because the loops in PgL, which connect helix α5 with either α4 or α6, are reorganized into helical structure upon opening of the lid thus increasing the length of α5. The C-terminal side of α4 and the

Figure 4

Comparison of the PcL (green) and PgL (red) structures. A stereo view displaying the structural rearrangement, involving helices α5 and α6 in the U1 domain, and the opening of helix α5 in PcL. The catalytic residue His286 is located behind helix α5 of PgL.

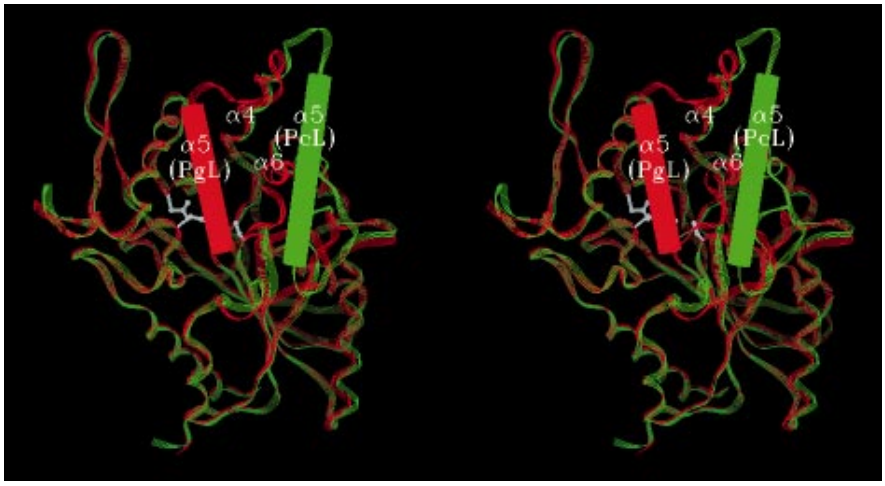

N-terminal side of α6 (in PgL) are melted into loops in PcL (Figs 1,4) and thus both helices are shorter in PcL by about half a turn. Only the C-terminal end of helix α4 (in PcL) shows some movement; in helix α6 (in PcL), the N-terminal side shows a greater movement than the C-terminal side. In PgL, the U1 domain fully buries the active site, whereas in PcL the active site becomes highly open to the solvent by the opening of the helical lid. In the recent structure of CvL [18], the lid is partially open but still the catalytic triad is not exposed to the solvent. These three structures may be associated with the different stages of a conformational transition which occurs during interfacial activation at an oil–water interface.

Some other structural changes of smaller magnitude also accompany the movement of the U1 domain (Figs 4,5). The second largest difference is observed in the 'oxyanion loop' encompassing residues 17–27 (marked A in Fig. 5), in which the oxyanion-forming residue Leu17 is included. The position of this loop in PgL corresponds roughly to the C-terminal side of helix α5 in PcL. The backbone nitrogen atom of Leu17 moves by 2.2 Å between PgL and PcL; this is much larger than the 0.7 Å shift occurring between PgL and CvL [18]. As a consequence of the structural rearrangement in this loop, a short antiparallel β sheet is newly formed in the PcL structure by the two short strands β1 and β2 (Fig. 3). The same β sheet is also present in the CvL structure [18]. The next largest structural difference occurs at residues 50–52 (marked B in Fig. 5), which contact the oxyanion loop as well as α5 and α6 in PcL. The movements of residues 50–52, the oxyanion loop, and the helical segment of α5 and α6 seem to be correlated. The difference between the structures of PcL and PgL in residues 233–234 (marked D in Fig. 5) results from the inserted residue, Val235. An intermolecular interaction with the U1 domain of the symmetry-equivalent molecule induces a small conformational change in the β hairpin of residues 219–222 (Fig. 5). In addition, strand β6 in PcL, one of the β strands composing the central β sheet, is characterized by being relatively longer than its equivalent in PgL (Fig. 1); β6 is also long in CvL [18]. As these homologous lipases share high sequence identity (84%) and similar structures of the main catalytic domain, it would be reasonable to assume that a conformational rearrangement, resulting from the opening of the helical lid, is in most part responsible for the observed structural differences between

Figure 5

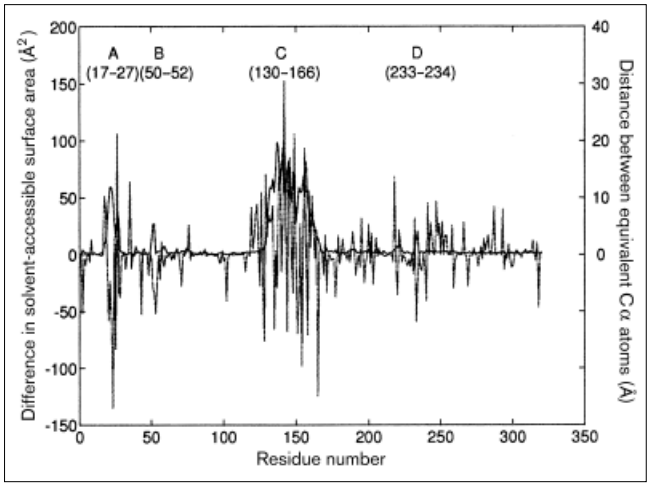

The difference in the solvent-accessible surface area (Å^2) for each residue and the distance (Å) between the structurally equivalent 318 Cα atoms of PcL and PgL are plotted against the residue number of PcL in dotted lines and solid lines, respectively. Four regions showing root mean square deviations of greater than 2.0 Å for Cα atoms are indicated: A, residues 17–27; B, residues 50–52; C, residues 130–166; D, residues 233–234.

Figure 6

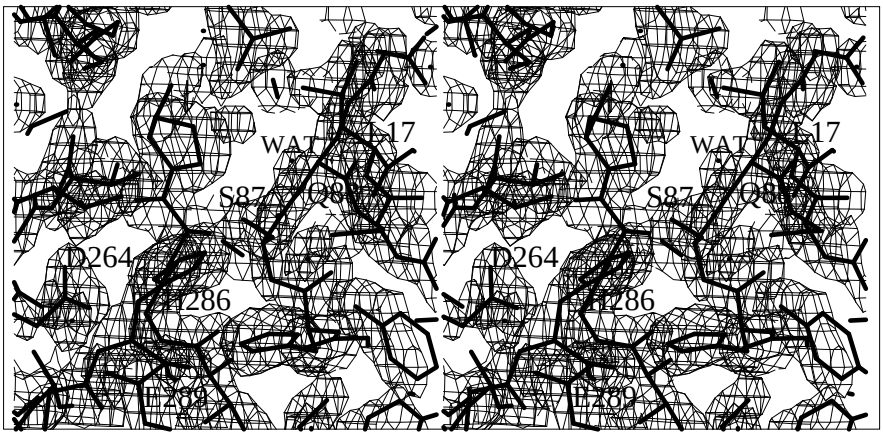

A stereo view of the catalytic triad and its vicinity with the ($2F_o$–F_c) electron density contoured at 1.2σ. Some residues and a water molecule (WAT) in the oxyanion hole are labeled.

them. Nevertheless, one should also consider the possible contributions of sequence differences to the structural differences observed. However, these contributions can only be a minor factor, because the homologous lipases of PcL, PgL, and CvL show a relatively uniform sequence conservation across the polypeptide chain.

When superimposed with the closed conformation of PgL, the recent crystal structure of CvL determined at 1.6 Å [18] has revealed several conformational differences. Large deviations are found for the three segments of residues 15–28, 49–54, and 128–158. These regions are virtually identical to the segments of PcL, which show large discrepancies in superimposition with PgL (Fig. 5). As the coordinates of CvL are not yet available, only a brief, visual comparison between the PcL and CvL structures is made here. In the CvL structure, helix α5 is moved slightly away from the active center, thus forming the oxyanion hole [18]. Therefore, the partially open conformation of the CvL structure probably represents an intermediate stage of the conformational transition from the closed state, as in PgL, to the highly open state, as in PcL. The conformational differences observed in the three crystal structures of highly similar lipases are likely to be associated with the activation at an oil–water interface. Thus this study, along with the previous results, provides a structural basis for understanding interfacial activation in bacterial lipases.

The catalytic triad and its vicinity

In PcL, three residues (Ser87, His286 and Asp264) located at the C-terminal edge of the central β sheet, form the catalytic triad (Figs 2,4,6). The catalytic residues have the same sequential order as those found in other α/β-hydrolases and the structure of the catalytic triad is virtually identical to those found in other α/β-hydrolases [20]. In PcL, the nucleophile, Ser87, is located on a sharp, γ-like turn between β3 and α3. The mainchain conformational angles for the catalytic Ser87 lie in a generously allowed region of the Ramachandran plot ($\phi = 51°$, $\psi = -128°$ for one molecule in the asymmetric unit and $\phi = 49°$, $\psi = -130°$ for the other molecule). Despite slightly unfavorable φ,ψ values, the region around Ser87 is well defined in the model with low B factors and a clear electron-density map (Fig. 6). Equivalent nucleophilic residues in other α/β-hydrolase fold enzymes have also been observed to lie in an unfavorable region of the Ramachandran plot [20]. The sequence around Ser87 (Gly-X-Ser-X-Gly) is found in many other serine hydrolases [43]. The position of the catalytic residue Ser87 at the end of a sharp turn allows His286 to gain easy access on one side and the substrate to gain access on the other. It was hypothesized that this special configuration of the nucleophile in the active site is essential for the hydrolysis of the substrate [20].

A calcium-binding site was readily located in PcL in the (F_o–F_c) difference Fourier and MIR maps, at a position equivalent to that in PgL. The calcium ion ligands are the two carboxylate groups of Asp242 and Asp288, two carbonyl groups of Gln292 and Val296, and two water molecules (Table 1). All the distances to calcium, with one exception,

Table 1

The calcium-binding site in *Pseudomonas cepacia* lipase.

Residue	Atom	B factor (Å²)*		Distance (Å)*	
		Mol 1	Mol 2	Mol 1	Mol 2
Calcium	Ca^{2+}	10.5	11.7		
Asp242	Oδ2	8.4	14.2	2.41	2.43
Asp288	Oδ1	9.9	8.5	2.41	2.34
Gln292	O	20.3	23.5	2.91	2.88
Val296	O	14.7	15.1	2.42	2.34
Wat507	OH2	3.0	7.0	2.28	2.28
Wat538	OH2	10.4	17.2	2.37	2.40

*Mol 1 and Mol 2 relate to the two molecules within the asymmetric unit.

Figure 7

A stereo view of the superposition of PcL (green), PgL (red), and CaL (blue) complexed with a phosphonate inhibitor (magenta). The active sites of PcL, PgL, and CaL are superimposed on the basis of the residues around the catalytic triads. The oxyanion hole present in the CaL structure is also formed in PcL, but not in PgL. The oxyanion hole is occupied by a water molecule in PcL, which is positioned close to the phosphonyl oxygen atom of the inhibitor in the CaL structure. Dashed lines represent hydrogen bonding or a strong ionic interaction between Ser87, His286, Asp264, Glu289, and His86, and hydrogen bonding between the water and backbone nitrogen atoms of Leu17 and Gln88.

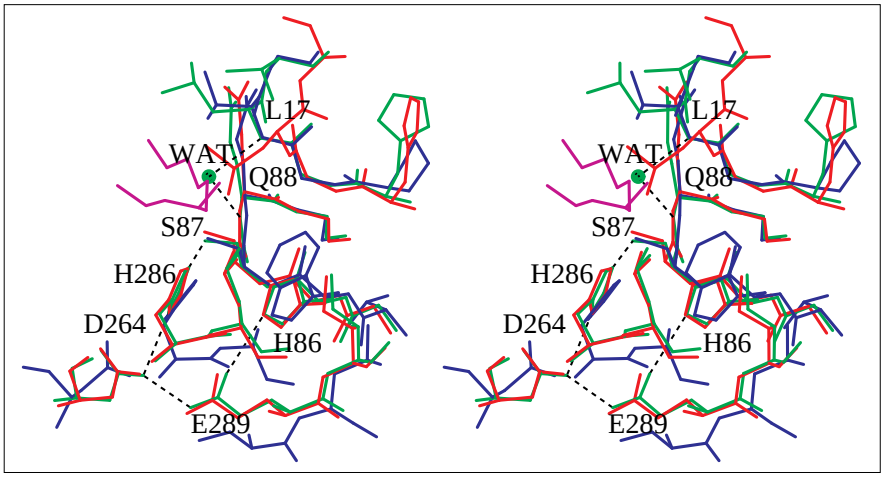

are about 2.4 Å. It is possible that the exceptionally long distance observed between Gln292 and the calcium ion may have been caused by the modeling of the peptide bond between Gln292 and Leu293 as *trans*. This peptide bond has been modeled as *cis* in the 1.6 Å structure of CvL [18]. Our refinement at a somewhat lower resolution of 2.1 Å is ambiguous in assigning a *cis* peptide bond. Six ligand oxygen atoms form a slightly distorted tetragonal bipyramid around the calcium ion: four oxygen atoms (from a water molecule, Asp242, Asp288, and Gln292) are almost co-planar and form a distorted square; two oxygen atoms (from a water and Val296) are located at both ends of the pyramid. The calcium-binding region is relatively rigid, reflected by the low B factors of the ligands and the calcium ion (Table 1). The catalytic residue His286, located in a loop where three calcium ligands (Asp288, Gln292, and Val296) are positioned, may be stabilized by calcium binding. In addition, Asn285 next to His286 makes a hydrogen bond with a water molecule which is one of the calcium ligands. Compared with the average B factor of 15.5 $Å^2$ for all atoms of the two lipase molecules in the asymmetric unit, relatively low B factors of His286 (9.6 $Å^2$ and 10.7 $Å^2$, respectively, for the two molecules) reflect the rigidity of this residue. As suggested in the PgL structure [17], and supported by a mutational study on Asp241 of PgL [40] (equivalent to Asp242 of PcL), the calcium binding near His286 may be necessary to stabilize the triad structure. A disulfide bond Cys190–Cys270 in PcL (and its equivalent in PgL) is not conserved among lipases but Cys270 (in helix α10) is positioned near the catalytic residue Asp264 in the nearby loop. The stabilization of helix α10 and a loop between α7 and β6′ by this disulfide bond may contribute to the rigidity of Asp264 in the triad.

One interesting feature of the active site in PcL is the presence of a network of polar residues around the catalytic triad. The Oδ2 atom of Asp264 makes a hydrogen bond with Nδ1 of His286 at a distance of 2.92 Å (Fig. 7). In addition, the Oε2 atom of Glu289 is close to the Oδ2 atom of Asp264 (2.58 Å); a similarly short distance (2.58 Å) is also observed in CvL [18]. The other carboxylic oxygen atom (Oε1) of Glu289 interacts with the Nε2 atom of His86 (3.05 Å). Therefore, five polar residues (Ser87, His286, Asp264, Glu289, and His86) interact among themselves within 3.1 Å (Fig. 7). The distance of 3.63 Å between the Oε1 atom of Glu289 and the Nε2 atom of His286 suggests the possibility of a potential interaction between them. This is supported by a mutational study on PgL. When Asp263 of PgL (equivalent to Asp264 of PcL) was mutated to alanine, the mutant retained 25% of its catalytic activity [38]. This observation indicates that Glu289 may play a role as an alternative proton acceptor when the catalytic Asp264 is replaced by alanine (Fig. 7).

The oxyanion hole

Previous crystallographic and biochemical studies have shown that the mechanism of hydrolysis by lipases is similar to that of serine proteases. In both cases, an oxyanion created during hydrolysis is located in the so-called 'oxyanion hole' and is stabilized through interactions with some electrophiles. A possible oxyanion hole in PcL has been deduced. The oxyanion hole was identified after some of the hydrogen bonds involved were recognized, following the superimposition of the active sites of PcL and CaL complexed with phosphonate inhibitor (Fig. 7). In this superposition, one water molecule in the PcL structure fills the oxyanion hole in the CaL structure. Two backbone nitrogen atoms, of Leu17 and Gln88 (Fig. 7), make hydrogen bonds to the water molecule in the oxyanion hole (2.89 Å to Leu17 and 3.07 Å to Gln88). No such oxyanion hole is present in the closed PgL structure [17]. Gln88 is preceded by the catalytic serine and the residue preceding

Figure 8

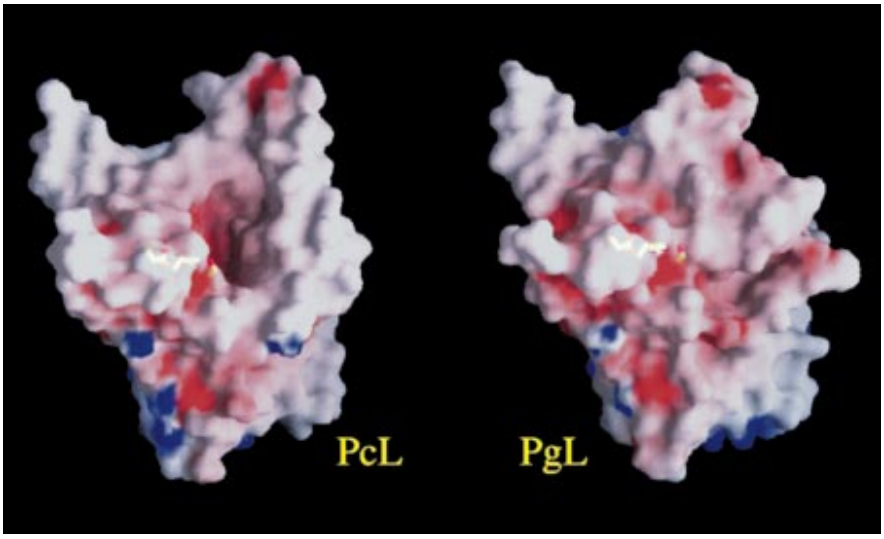

A comparison of the molecular surfaces of PcL and PgL. The catalytic residues of the two lipases have been superimposed so as to view the active sites in the same orientation. The active-site cleft, exposed to the solvent in the open conformation of PcL, is completely buried in the closed conformation of PgL. The molecular surface is drawn with half transparency and the catalytic residues in PcL and PgL are only faintly visible; negatively charged regions are shown in red, positively charged regions are in blue. (Figure drawn with the program GRASP [61].)

Leu17 is glycine, as in several other lipases or esterases [44]. For PgL, one of the residues forming the oxyanion hole was mistakenly listed as Ala18 [44]. The residue Leu17 is at the C-terminal end of β1 in PcL (corresponding to β3 in the general α/β-hydrolase fold). When compared with the closed structure of PgL, in PcL the loops at the C-terminal ends of β1 and β2 change their positions and make new contacts with the opened U1 domain (Figs 4,5). Following these conformational changes, Leu17 in the loop between β1 and α1 moves to a position near the nucleophile Ser87 and forms the oxyanion hole. As found in *R. miehei* lipase (RmL) [45], *H. lanuginosa* lipase (HlL) [30], and the human pancreatic lipase–porcine colipase complex [46], the oxyanion hole in PcL is not preformed but is generated by the opening of the lid. However, the catalytic triads of PcL and PgL in different conformations are virtually superimposable (Fig. 7). In the partially open conformation of CvL [18], with the lid starting to move away from the active site, the oxyanion hole is already formed by the amide nitrogen atoms of Leu17 and Gln88. It is interesting to note that cutinase, a lipolytic enzyme without a lid and not displaying interfacial activation, has a preformed oxyanion hole [47].

The active-site structure in the open conformation

In comparison with the closed structure of PgL [17] and the partially open structure of CvL [18], helix α5 of the U1 domain in the present open structure of PcL is rolled up to expose both a large deep active-site cleft and the catalytic residues to the solvent. The flat bottom of the exposed cleft is formed by the C-terminal loops from the central six-stranded β sheet and is encompassed by two-sided walls, constructed from both the U1 and U2 domains (Figs 2,4). In PcL a deep pocket is found in the center of the large active-site cleft, this pocket is approximately 7 Å×17 Å wide and approximately 8 Å deep from the flat surface of the cleft to the Cα atom of Ser87 (Fig. 8); Ser87 is located in the middle of the pocket. In PgL, this pocket remains largely unchanged but is shielded from the solvent by the closed U1 domain. The pocket and the active-site cleft around it are rich in hydrophobic residues. No strong electron densities corresponding to detergent molecules are observed in this pocket of PcL. A negatively charged surface around the nucleophile, Ser87, (Fig. 8) may be required to remove the negatively charged product, a fatty acid, from this pocket after hydrolysis, as is also found in CrL and CaL [6,13].

The nucleophilic Ser87, located in the middle of the active-site cleft (Figs 2,4), is accessible only from one side of the cleft (the β1 side). The other side of the cleft (the β6 side) is narrow and nearly blocked by the sidechain atoms. The rearrangement of the U1 domain changes the nature of the molecular surface. When the difference in the solvent-accessible surface area of each residue between PcL and PgL is plotted against the residue number (Fig. 5), the pronounced differences are localized to the same regions of the structure where large conformational changes take place. The opening of the lid increases the total molecular surface area by 520 $Å^2$, amounting to 4.4% of the total surface area of the PgL structure (Figs 5,8). This value is nearly eight times larger than that of 66 $Å^2$ as observed for CvL in comparison with PgL [18]. As shown in Figure 5, the difference in the solvent-accessible surface area for each residue varies from positive to negative values. This reflects the fact that the lid in the open state is stabilized not only by the hydrophobic environment but also by the intramolecular contacts themselves. The areas encompassing regions A and B in Figure 5 (residues 17–27 and 50–52, respectively) are decreased by 370 $Å^2$ in PcL

Figure 9

A stereo view of the Cα trace of PcL (green) and its symmetry-related molecule (red). The sidechains of hydrophobic residues within the U1 domain (Phe119, Phe122, Val123, Val126, Val129, Pro131, Thr132, Leu134, and Leu139) and a residue of the U2 domain (Val254), shown in magenta, interact with residues located in the U2 domain of the symmetry-related molecule (Ile218, Leu234, Val235, Pro237, Ala240, Leu241, Leu246, Phe249, Gly250, and Thr253), shown in blue. Some Cα positions in the U1 and U2 domains are labeled. The residues of the catalytic triad (Ser87, His286, and Asp264) are shown in purple.

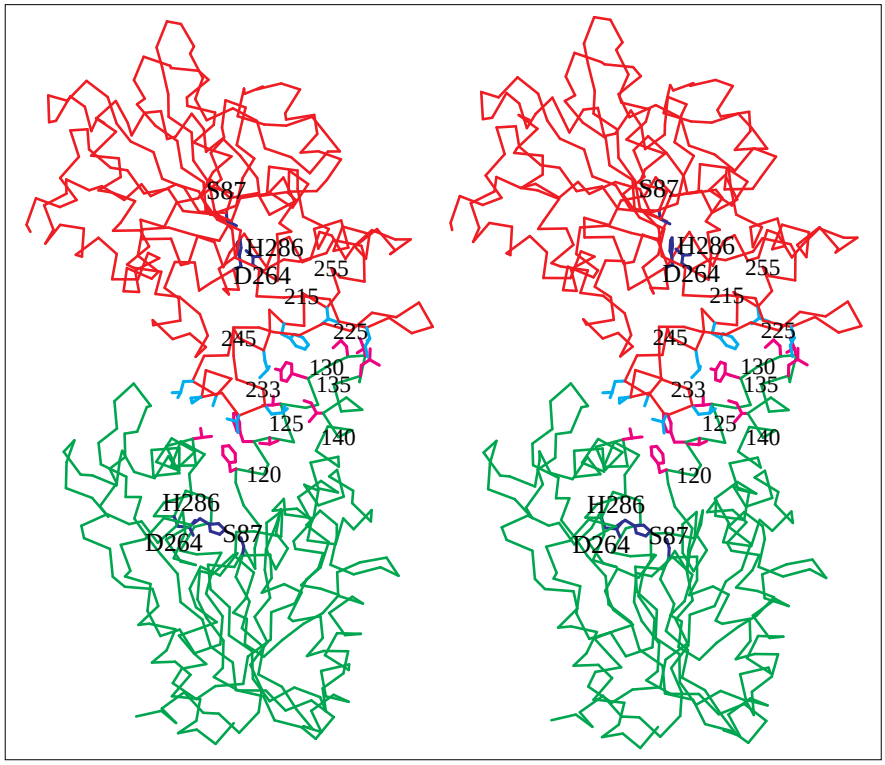

compared to PgL. This observation indicates that these loop regions are rearranged in such a way that tight intramolecular contacts are possible in the new environment after opening of the lid. This change in surface area is caused not only by exposing the active-site cleft and the hydrophobic inside surface of the U1 domain but also by the appearance of a pocket which may be the substrate-binding site (Fig. 8).

Lipase opening and crystal packing

In PgL, the B factors of α5 and the loop at its C-terminal end are extremely high; this region was proposed as a candidate for the lid [17]. In PcL, the average B factor of the U1 domain, which shows the largest movement, is only slightly higher than that of the whole protein (19.8 Å^2 versus 15.5 Å^2 for residues 130–166). The open conformation of the U1 domain in this structure is possibly stabilized in part by crystal-packing forces. The exposed hydrophobic residues, from the inside of the U1 domain of PcL, make distant van der Waals interactions with hydrophobic residues from the U2 domain (β3, β4, α8, and α9) of the symmetry-related molecule (Fig. 9). The surface area as far as 830 Å^2 from the U1 domain is in contact with the symmetry-related molecule. Additional hydrophilic interactions between the outside of the U1 domain and the C domain also contribute to stabilizing the open U1 domain.

The fully or partially open conformations of other lipases have been determined in the absence of an inhibitor bound to the active site, these lipases include CvL [18], CrL [11], and the lipase form *Rhizopus delemar* (RdL). In the crystal structure of RdL, the two molecules in the asymmetric unit showed different lid conformations [29]: one of them is closed and the other is in an intermediate state between the open and closed forms. All these lipase crystals obtained in the open conformation were grown in the presence of 2-methyl-2,4-pentanediol (MPD) [11,18,30,38]. It seems likely that this specific crystallization medium may exert a positive influence on stabilizing the open conformation of lipases. In the case of CrL and RdL, similarly to PcL, the open lids are stabilized by intramolecular contacts as well as by intermolecular interactions with symmetry-related molecules in the crystals. The stable open conformation adopted by lipases in the absence of a bound substrate or its analog indicates that the crystal-packing forces may play a considerable role in selectively stabilizing certain conformations. In addition, the disordered lid domains in the structures of HlL and CaL, where the lids are free from intermolecular interactions within crystals [12,13], stress the important role of crystal packing. The open conformations of lipases have also been observed when crystallized in the presence of an inhibitor or a substrate analog bound to the active site, with or without the addition of detergent micelles [15,45,46,48].

A comparison with less homologous lipases

PcL has a typical α/β-hydrolase fold in the C domain, comprised of six parallel β strands and six α helices, with two smaller domains (U1 and U2) being inserted into the C domain. When compared with *Geotrichum candidum* lipase and CrL, PcL appears to have the same essential part of the α/β-hydrolase fold, which is necessary for the catalytic activity. The location of the catalytic aspartic acid residue is, however, different from other lipases. In the typical α/β-hydrolase fold, an aspartic acid residue in the catalytic triad is usually found within the C-terminal end of β7, and the second insertion follows this catalytic residue. In contrast, the catalytic residue, Asp264, in PcL is located between the second insertion and α10 (equivalent to αE in the general α/β-hydrolase fold [20]). The sharp and bulged β turn in the U2 domain, observed in both structures of PcL and PgL, is an unusual feature among lipases. As it is reasonable to assume that both PcL and PgL have homologous structures owing to their high sequence identity, the different conformations provide indirect evidence for the kind of motion occuring during interfacial activation. In the case of PcL (and PgL), a relatively large number of residues (37; residues 130–166) out of 320 residues, are involved in the opening of the lid, as compared with 29 (residues 65–93) out of 525 in CrL and 14 (residues 82–95) out of 269 in RmL. As a consequence of such a large scale movement, the active site of PcL becomes highly accessible to the solvent. The *cis/trans* isomerization of a proline residue, which occurs during the opening of the lid in CrL [11], is not observed in PcL.

The active site of PcL shows all the characteristics which are known to be conserved among lipases. The same principle of activation mechanism may be applied to PcL as well as to other lipases. The catalytic triad and the structural features of PcL created by the opening of the lid, such as the formation of an oxyanion hole and the exposure of a substrate-binding pocket, are well conserved in the open structures of other lipases, such as CrL, RmL, and CaL [6,7,27]. The similar consequences of the conformational changes strongly suggest that the open conformation of PcL observed in this study represents an active state, whereas the closed conformation of PgL represents an inactive state. All the structural data provided by this study support the view that PcL shares the same mechanisms of interfacial activation and catalytic action with other lipases.

Biological implications

Lipases catalyze the hydrolysis of triacylglycerides and their activity is drastically enhanced at an oil–water interface. They are widely used as catalysts for stereospecific hydrolysis or organic synthesis, because they display strong stereospecificity on chiral substrates.

The crystal structure of *Pseudomonas cepacia* lipase (PcL) reported here shows many structural similarities to other lipases, such as an **α/β**-hydrolase fold and the Ser-His-Asp catalytic triad. However, there are some unusual features in the structure of PcL (these features are also found in two homologs of PcL, from *Pseudomonas glumae*, PgL, and *Chromobacterium viscosum*, CvL). One of these features is a calcium site, which supposedly stabilizes the catalytic triad. This is different from the case of human pancreatic lipase in which a calcium ion, located remotely from the active site, appears to play a purely structural role in stabilizing the conformation of a surface segment. Another novel feature of PcL is the presence of an additional carboxylic acid which may serve as an alternative proton acceptor in the catalytic triad.

The most remarkable feature in the present structure of PcL, as compared to the closed structure of PgL and the partially open structure of CvL, is the highly open conformation. Upon opening of the so-called 'lid' region, a relatively large active-site cleft is exposed to the solvent in PcL. This conformational change involves mainly two helices, one of which covers the active sites in both the PgL and CvL structures. An oxyanion hole, not formed in the closed structure of PgL but present in the partially open structure of CvL, is also formed in the highly open structure of PcL. The observed structural changes are likely to be associated with the interfacial activation which occurs in lipolysis. The open conformation adopted by PcL in the present crystal, which was grown in the presence of 2-methyl-2,4-pentanediol, may be stabilized in part by the crystal-packing forces. The present open structure of PcL, together with the previously reported structures of PgL and CvL, provides an insight into understanding the process of interfacial activation in bacterial lipases.

Materials and methods

Purification, crystallization, and preparation of heavy-atom derivatives

The protein used for crystallization was purified by gel filtration from crude lipase purchased from Amano Pharmaceutical Co., Ltd. (Lipase PS AMANO, LPSA001526) [38]. Crystallization was achieved by the hanging-drop vapor diffusion method at room temperature, as described previously [38]. Isomorphous heavy-atom derivative crystals were prepared by soaking the native crystals into mother liquor containing the specified concentration of heavy-atom compounds (Table 2).

Data collection and processing

X-ray diffraction data of native and all heavy-atom derivatives were collected at 18°C on a FAST area detector system (Enraf-Nonius) using the MADNES software [49]. Graphite-monochromatized CuKα X-rays from a rotating-anode generator (Rigaku RU-200), running at 40 kV and 70 mA were used with 0.3 mm focus cup and 0.6 mm collimator. The reflection intensities were obtained by the profile-fitting procedure [50] and the data were scaled by the Fourier scaling program [51].

The reflections were indexed on a primitive monoclinic lattice with corresponding unit cell parameters of a = 85.23 Å, b = 47.42 Å, c = 86.53 Å, and β = 116.11° by the autoindexing and parameter refinement procedure in MADNES software; the space group was determined to be $P2_1$ [38]. The merged native data set consisted of 106 596 measurements

Table 2

Data collection and heavy-atom refinement statistics.

Compound	Concentration (mM)	Time (days)	Resolution (Å)	No. of reflections	Completeness (%)	R_{sym}* (%)	R_{deriv}† (%)	No. of sites	Phasing‡ power	R_{cullis}§
Native			2.06	29 375	80.0	4.0				
K_2PtBr_4	20	10	2.41	18 826	77.2	3.3	25.3	8	1.9	0.58
Na_2PtCl_4	30	20	2.41	19 438	79.7	3.6	34.8	6	1.6	0.62
$Pt(NH_3)_2(NO_2)_2$	35	8	2.39	20 076	80.4	3.8	34.5	8	1.1	0.79
$Pt(NH_2)_2Cl_2$	20	40	2.40	18 583	74.4	4.0	27.1	6	1.9	0.58
$PhHgCH_3COO$	30	3	2.31	22 916	83.0	3.5	13.4	8	0.7	0.84
PhHgOH	5	10	2.41	18 912	77.6	4.3	15.7	18	0.9	0.81

*$R_{sym} = \Sigma|I - \langle I \rangle| / \Sigma \langle I \rangle$. †$R_{deriv} = \Sigma(|Fph - Fp|) / \Sigma Fp$. ‡Phasing power = $[\Sigma|Fh|^2 / \Sigma(|Fph(obs)| - |Fph(calc)|)^2]^{1/2}$.
§$R_{cullis} = \Sigma||Fph \pm Fp| - Fph(calc)| / \Sigma|Fph \pm Fp|$. The figure of merit calculated for 22 868 reflections within the resolution range 20.0–2.3 Å = 0.57.

of 29 375 unique reflections with an R_{merge} (on intensity) of 4.0% (rejecting 2.7% outliers), the data completeness was 80.0% between 30.0 Å and 2.06 Å (34% complete between 2.2 Å and 2.1 Å). For two molecules (Mr 33 128) in the asymmetric unit (or four molecules in each unit cell), the V_M value is 2.35 Da Å^3, corresponding to a solvent content of 48% [52]. The two molecules in the asymmetric unit were found to be related by an approximate translation of Y = ½ by the native Patterson map and this is also consistent with the pseudo C2 symmetry of diffraction intensity distribution. The present work employed the $P2_1$ space group for both phase determination and model refinement. (Both space groups C2 and $P2_1$ give essentially indistinguishable results up to about 2.4 Å for all practical purposes but beyond that the latter gives a better R factor in refinement.) For the collection of the heavy-atom derivative data set, only partial diffraction data covering about a 10° rotation was obtained and compared with the native data. Data collection was continued for the derivative crystals, when the scaling R factor [51] was above 10% and cell parameter changes were within 0.5%. A summary of the data collection is given in Table 2.

Table 3

Statistics for crystallographic refinement.

Resolution of data (Å)	8.0–2.1
Number of reflections with $F > 2\sigma_F$ (all)	28 405
Number of reflections with $F > 2\sigma_F$ (test)	2 828
R factor (%)*	18.7
Free R factor (%)†	25.5
Number of protein atoms excluding hydrogen‡	2 337 × 2
Number of calcium ions	2
Number of waters	398
Root mean square deviations	
bond distances (Å)	0.011
angle distances (°)	1.68
dihedral angles (°)	24.23
improper angles (°)	1.63
B factors for bonded atoms (Å^2)	2.6
Average B factors (Å^2)	
mainchain atoms	14.9
sidechain atoms	16.3
waters	42.0
calcium ions	11.1
all atoms	17.6

*R factor = $\Sigma||F_{calc}| - |F_{obs}|| / \Sigma|F_{obs}| \times 100$, where F_{calc} and F_{obs} are the calculated and observed structure factor amplitudes, respectively. †A small fraction (10%) of reflections were randomly selected and used to calculate the free R factor. ‡There are two molecules in the asymmetric unit and each lipase molecule contains 2337 non-hydrogen atoms.

Molecular replacement

A search model for molecular replacement was constructed from the previously reported structure of the homologous lipase, PgL [17]. After rotation and translation searches, and a subsequent rigid-body refinement with the program package AMoRe [53], the best solution gave an R factor of 43.3% and a correlation coefficient of 0.697 for the 15–4.0 Å data. However, several trials of subsequent crystallographic refinement and model rebuilding failed to produce a satisfactory model, with the crystallographic R factor remaining around 25% and the electron density for the segment surrounding the active site (corresponding to residues 120–160) remaining obscure. The cause of this difficulty turned out to be the different conformations of the two lipases.

MIR phasing

As the molecular replacement model could not be refined to a satisfactory R factor, we decided to use the heavy-atom derivative data to obtain independent phase information by MIR. A difference Patterson map of the K_2PtBr_4 derivative calculated with 20–4.0 Å data was interpreted using a graphical method of determining the heavy-atom positions in the CCP4 program package [54]. Heavy-atom sites of other derivatives were located in the difference Fourier map calculated with the K_2PtBr_4-derived MIR phases. The heavy-atom positions were also verified in the difference Fourier maps calculated with the model phases from the molecular replacement. Refinement of heavy-atom parameters and calculation of MIR phases to 2.6 Å were performed with the program MLPHARE [54] (Table 2).

Density modification, map calculation, and phase combination

Initial phases were improved by solvent flattening and histogram matching with the program DM in the CCP4 package [54]. The initial molecular envelope was built from the model obtained from the molecular replacement method and new envelopes were reconstructed from the partial models in each refinement step. Phases computed from the improved maps or partial models were combined with the experimental MIR phases in each cycle of refinement with the program SIGMAA [54]. SIGMAA-weighted ($2mF_o - DF_c$) maps in each refinement cycle showed considerable improvements.

Model building and refinement

Model building was performed with the program O [55] on a Silicon Graphics workstation. For the sake of convenience, the partially-refined model from molecular replacement was rebuilt using both MIR and density-modified maps. The refinement started with a rigid-body refinement at 3.0 Å. All refinements were performed using the program X-PLOR [56] with the stereochemical parameters of Engh and Huber [57]. The positional refinement started with data between 8 and 2.7 Å with $2\sigma_F$ cut-off and the resolution was gradually extended to 2.1 Å. SIGMAA-weighted ($2mF_o - DF_c$) maps calculated with the combined phases permitted the detection of all structural differences between PcL and PgL, and modeling of all ambiguous parts in the initial model.

Molecular dynamics refinement with simulated annealing was performed for each cycle from 3000 to 300K, with a time step of 0.5 fs, followed by 120 cycles of positional refinement. After the R factor was reduced below 24%, some peaks above at least 3.5σ in the (F_o–F_c) electron-density map were selected as candidates for the calcium ion and water molecules. The non-crystallographic symmetry between the two independent molecules in the asymmetric unit was released only at the final stage of the refinement. The individual B factors were refined using 2.1 Å data.

Model quality and accuracy

The refined model gives an R factor of 18.7% for 8.0–2.1 Å data (28 405 reflections with $F > 2\sigma_F$) with a free R factor of 25.5% (2 828 reflections). It comprises all 640 residues of the two lipase molecules, 398 waters, and two calcium ions in the asymmetric unit. Structural evaluation with the program PROCHECK [58] indicates that the refined structure has good geometric parameters (Table 3). For each lipase molecule three residues lie in the generously-allowed regions of the Ramachandran plot [59] (Thr18, Ser87, Leu293) and one in the disallowed regions (Leu234). An example of the final ($2F_o$–F_c) electron-density map calculated with the model phases is given in Figure 6.

Accession numbers

The coordinates and structure factor data have been deposited with the Protein Data Bank with accession codes 1OIL and R1OILSF, respectively.

Acknowledgements

We thank MEM Noble and LN Johnson for supplying the coordinates of PgL, and D Ollis, Y Kim, and CH Chang for comments and assistance. We also thank the Korea Ministry of Education (International Cooperative Research Program), the Center for Molecular Catalysis, the Korea Sanhak Foundation, and the Basic Sciences Research Institute, MOE, (BSRI-96-3418) for financial support. The publication cost was supported in part by the Research Institute of Molecular Science. The X-ray equipment was provided by the Inter-University Center for Natural Science Research Facilities at Seoul National University. The X-ray equipment was supported in part by the Korea Science Engineering Foundation Specialization Support Fund.

References

1. Borgström, B. & Brockman, H.L. (1984). *Lipases*. Elsevier, Amsterdam, Netherlands.
2. Santaniello, E., Ferraboschi, P., Grisenti, P. & Manzocchi, A. (1992). The biocatalytic approach to the preparation of enantiomerically pure chiral building blocks. *Chem. Rev.* **92**, 1071–1140.
3. Tramper, J., van der Plas, H.C. & Linko, P. (1985). *Biocatalysts in Organic Syntheses*. Elsevier, Amsterdam, Netherlands.
4. Kazlauskas, R.J., Weissfloch, A.N.E., Rappaport, A.T. & Cuccia, L.A. (1991). A rule to predict which enantiomer of a secondary alcohol reacts faster in reactions catalyzed by cholesterol esterase, lipase from *Pseudomonas cepacia*, and lipase from *Candida rugosa*. *J. Org. Chem.* **56**, 2656–2665.
5. Cygler, M., *et al.*, & Gupta, A.K. (1994). A structural basis for the chiral preference of lipases. *J. Am. Chem. Soc.* **116**, 3180–3186.
6. Grochulski, P., *et al.*, & Cygler, M. (1994). Analogs of reaction intermediates identify a unique substrate binding site in *Candida rugosa* lipase. *Biochemistry* **33**, 3494–3500.
7. Uppenberg, J., *et al.*, & Jones, T.A. (1995). Crystallographic and molecular-modeling studies of lipase B from *Candida antarctica* reveal a stereospecificity pocket for secondary alcohols. *Biochemistry* **34**, 16838–16851.
8. Brady, L., *et al.*, & Menge, U. (1990). A serine protease triad forms the catalytic center of a triacylglycerol lipase. *Nature* **343**, 767–770.
9. Schrag, J.D. & Cygler, M. (1993). 1.8 Å refined structure of the lipase from *Geotrichum candidum*. *J. Mol. Biol.* **230**, 575–591.
10. Schrag, J.D., Li, Y., Wu, S. & Cygler, M. (1991). Ser-His-Glu triad forms the catalytic site of the lipase from *Geotrichum candidum*. *Nature* **351**, 761–764.
11. Grochulski, P., *et al.*, & Cygler, M. (1993). Insights into interfacial activation from an open structure of *Candida rugosa* lipase. *J. Biol. Chem.* **268**, 12843–12847.
12. Derewenda, U., *et al.*, & Derewenda, Z.S. (1994). An unusual buried polar cluster in a family of fungal lipases. *Nat. Struct. Biol.* **1**, 36–47.
13. Uppenberg, J., Hansen, M.T., Patkar, S. & Jones, T.A. (1994). The sequence, crystal structure determination and refinement of two crystal forms of lipase B from *Candida antarctica*. *Structure* **2**, 293–308.
14. Winkler, F.K., D'Arcy, A. & Hunziker, W. (1990). Structure of human pancreatic lipase. *Nature* **343**, 771–774.
15. van Tilbeurgh, H., Egloff, M.-P., Martinez, C., Rugani, N., Verger, R. & Cambillau, C. (1993). Interfacial activation of the lipase–procolipase complexes by mixed micelles revealed by X-ray crystallography. *Nature* **362**, 814–820.
16. Bourne, Y., Martinez, C., Kerfelec, B., Lombardo, D., Chapus, C. & Cambillau, C. (1994). Horse pancreatic lipase: the crystal structure refined at 2.3 Å resolution. *J. Mol. Biol.* **238**, 709–732.
17. Noble, M.E.M., Cleasby, A., Johnson, L.N., Egmond, M.R. & Frenken, L.G.J. (1993). The crystal structure of triacylglycerol lipase from *Pseudomonas glumae* reveals a partially redundant catalytic aspartate. *FEBS Lett.* **331**, 123–128.
18. Lang, D., *et al.*, & Schomburg, D. (1996). Crystal structure of a bacterial lipase from *Chromobacterium viscosum* ATCC 6918 refined at 1.6 Å resolution. *J. Mol. Biol.* **259**, 704–717.
19. Batenburg, A.M., Egmond, M.R., Frenken, L.G. & Verrips, C.T. (1991). Enzymes and enzymatic detergent compositions. European Patent 0 407 225 A1.
20. Ollis, D.L., *et al.*, & Goldman, A. (1992). The α/β hydrolase fold. *Protein Eng.* **5**, 197–211.
21. Pathak, D., Ngai, K.-L. & Ollis, D. (1988). X-ray crystallographic structure of dienelactone hydrolase at 2.8 Å. *J. Mol. Biol.* **204**, 435–445.
22. Sussman, J.L., *et al.*, & Silman, I. (1991). Atomic structure of acetylcholinesterase from *Torpedo californica*: a prototypic acetylcholine-binding protein. *Science* **253**, 872–879.
23. Franken, S.M., Rozeboom, H.J., Kalk, K.H. & Dijkstra, B.W. (1991). Crystal structures of haloalkane dehalogenase: an enzyme to detoxify halogenated alkanes. *EMBO J.* **10**, 1297–1302.
24. Liao, D.I., Breddam, K., Sweet, R.M., Bullock, T. & Remington, S.J. (1992). Refined atomic model of wheat serine carboxypeptidase II at 2.2 Å resolution. *Biochemistry* **31**, 9796–9812.
25. Martinez, C., Geus, P.D., Lauwereys, M., Matthyssens, G. & Cambillau, C. (1992). *Fusarium solani* cutinase is a lipolytic enzyme with a catalytic serine accessible to solvent. *Nature* **356**, 615–618.
26. Lawson, D.M., *et al.*, & Derewenda, Z.S. (1994). Structure of a myristoyl-ACP-specific thioesterase from *Vibrio harveyi*. *Biochemistry* **33**, 9382–9388.
27. Ghosh, D., *et al.*, & Duax, W.L. (1995). Structure of uncomplexed and linoleate-bound *Candida cylindracea* cholesterol esterase. *Structure* **3**, 279–288.
28. Brzozowski, A.M., *et al.*, & Thim, L. (1991). A model for interfacial activation in lipase from the structure of a fungal lipase–inhibitor complex. *Nature* **351**, 491–494.
29. Grochulski, P., Li, Y., Schrag, J.D. & Cygler, M. (1994). Two conformational states of *Candida rugosa* lipase. *Protein Sci.* **3**, 82–91.
30. Derewenda, U., *et al.*, & Derewenda, Z.S. (1994). Conformational lability of lipases observed in the absence of an oil–water interface: crystallographic studies of enzymes from the fungi *Humicola lanuginosa* and *Rhizopus delemar*. *J. Lipid Res.* **35**, 524–534.
31. Nakanishi, Y., Kurono, Y., Koide, Y. & Beppu, T. (1994). Recombinant DNA, bacterium of the genus *Pseudomonas* containing it, and process for preparing lipase by using it. United States Patent 5,290,694.
32. Jørgensen, S., Skov, K.W. & Diderichsen, B. (1991). Cloning, sequence, and expression of a lipase gene from *Pseudomonas cepacia*: lipase production in heterologous hosts requires two *Pseudomonas genes*. *J. Bacteriol.* **173**, 559–567.
33. Dunhaupt, A., Lang, S. & Wagner, F. (1991). Properties and purification of a *Pseudomonas cepacia* lipase. In *Lipase; Structure, Mechanism, and Genetic Engineering*. (Alberghina, L., Schmid, R.D., & Verger, R., eds), pp. 389–392, GBF monographs, VCH, Weinheim, Germany.
34. Kordel, M., Hofmann, B., Schomburg, D. & Schmid, R. D. (1991). Extracellular lipase of *Pseudomonas sp.* strain ATCC 21808: purification, characterization, crystallization, and preliminary X-ray diffraction data. *J. Bacteriol.* **73**, 4836–4841.
35. Nishioka, T., *et al.*, & Oda, J. (1991). Lipase from *Pseudomonas* sp.: reactions, cloning and amino acid sequence analysis. In *Lipase; Structure, Mechanism, and Genetic Engineering*. (Alberghina, L., Verger, R., Schmid, R., eds), pp. 253–262, VCH, Weinheim, Germany.

36. Sugihara, A., Ueshima, M., Shimada, Y., Tsunasawa, S. & Tominaga, Y. (1992). Purification and characterization of a novel thermostable lipase from *Pseudomonas cepacia*. *J. Biochem.* 112, 598–603.
37. Bornscheuer, U., *et al*., & Menge, U. (1994). Lipase of *Pseudomonas cepacia* for biotechnological purpose: purification, crystallization and characterization. *Biochim. Biophys. Acta* 1201, 55–60.
38. Kim, K.K., *et al*., & Suh, S.W. (1992). Crystallization and preliminary X-ray crystallographic analysis of lipase from *Pseudomonas cepacia*. *J. Mol. Biol.* 227, 1258–1262.
39. Weissfloch, A. & Kazlauskas, A. (1995). Enantiopreference of lipase from *Pseudomonas cepacia* toward primary alcohols. *J. Org. Chem.* 60, 6959–6969.
40. Frenken, L.G.J., Egmond, M.R., Batenburg, A.M., Bos, J.W., Visser, C. & Verrips, C.T. (1992). Cloning of the *Pseudomonas glumae* lipase gene and determination of the active site residues. *Appl. Environ. Microbiol.* 58, 3787–3791.
41. Aoyama, S., Yoshida, N. & Inouye, S. (1988). Cloning, sequencing and expression of the lipase gene from *Pseudomonas fragi* IFO-12049 in *E. coli*. *FEBS Lett.* 242, 36–40.
42. Tan, Y. & Miller, K.J. (1992). Cloning, expression, and nucleotide sequence of a lipase gene from *Pseudomonas fluorescens* B52. *Appl. Environ. Microbiol.* 58, 1402–1407.
43. Brenner, S. (1988). The molecular evolution of genes and proteins: a tale of two serines. *Nature* 334, 528–530.
44. Kazlauskas, R.J. (1994). Elucidating structure-mechanism relationships in lipases: prospects for predicting and engineering catalytic properties. *Trends Biotechnol.* 12, 464–472.
45. Derewenda, U., Brzozowski, A.M., Lawson, D.M. & Derewenda, Z.S. (1992). Catalysis at the interface: the anatomy of a conformational change in a triglyceride lipase. *Biochemistry* 31, 1532–1541.
46. Egloff, M.-P., Marguet, F., Buono, G., Verger, R., Cambillau, C. & van Tilbeurgh, H. (1995). The 2.46 Å resolution structure of the pancreatic lipase–colipase complex inhibited by a C11 alkyl phosphonate. *Biochemistry* 34, 2751–2762.
47. Martinez, C., *et al*., & Cambillau, C. (1994). Cutinase, a lipolytic enzyme with a preformed oxyanion hole. *Biochemistry* 33, 83–89.
48. Hermoso, J., Pignol, D., Kerfelec, B., Crenon, I., Chapus, C. & Fontecilla-Camps, J.C. (1996). Lipase activation by nonionic detergents. *J. Biol. Chem.* 271, 18007–18016.
49. Messerschmidt, A. & Pflugrath, J.W. (1987). Crystal orientation and X-ray pattern prediction routines for area-detector diffractometer systems in macromolecular crystallography. *J. Appl. Cryst.* 20, 306–315.
50. Kabsch, W. (1988). Evaluation of single-crystal X-ray diffraction data from a position-sensitive detector. *J. Appl. Cryst.* 21, 916–924.
51. Weissman, L. (1982). Strategies for extracting isomorphous and anomolous signals. In *Computational Crystallography*. (Sayre, D., ed.), pp. 56–63, Oxford University Press, Oxford, UK.
52. Matthews, B.W. (1968). Solvent content of protein crystals. *J. Mol. Biol.* 33, 491–497.
53. Navaza, J. (1994). AMORE: an automated package for molecular replacement. *Acta Cryst. A* 50, 157–163.
54. Collaborative Computing Project No. 4. (1994). The CCP4 suite: programs for protein crystallography. *Acta Cryst. D* 50, 760–763.
55. Jones, T.A., Zou, J.-Y., Cowan, S.W. & Kjeldgaard, M. (1991). Improved methods for building protein models in electron density maps and the location of errors in these models. *Acta Cryst. A* 47, 110–119.
56. Brünger, A.T. (1993). *X-PLOR, Version 3.1. A System for X-ray Crystallography and NMR*. Yale University Press, New Haven, CT.
57. Engh, R.A. & Huber, R. (1991). Accurate bond and angle parameters for X-ray protein structure refinement. *Acta Cryst. A* 47, 392–400.
58. Laskowski, R.A., MacArthur, M.W., Moss, D.S. & Thornton, J.M. (1993). PROCHECK: a program to check the stereochemical quality of protein structures. *J. Appl. Cryst.* 26, 283–291.
59. Ramachandran, G.N. & Sasisekharan, V. (1968). Conformation of polypeptides and proteins. *Adv. Protein Chem.* 23, 283–437.
60. Kraulis, P.J. (1991). MOLSCRIPT: a program to produce both detailed and schematic plots of protein structures. *J. Appl. Cryst.* 24, 946–950.
61. Nicholls, A., Sharp, K.A. & Honig, B. (1991). Protein folding and association: insights from the interfacial and thermodynamic properties of hydrocarbons. *Proteins* 11, 281–293.